Graph Filters and the Z-Laplacian

Xiaoran Yan

Indiana University Network Science Institute

Bloomington, IN 47408

Email: xiaoran.a.yan@gmail.com

Brian M. Sadler, Robert J. Drost, Paul L. Yu

Army Research Laboratory

Adelphi, MD 20783

Kristina Lerman

Information Science Institute, University of Southern California

Marina Del Rey, CA 90292

Abstract

In network science, the interplay between dynamical processes and the underlying topologies of complex systems has led to a diverse family of models with different interpretations. In graph signal processing, this is manifested in the form of different graph shifts and their induced algebraic systems. In this paper, we propose the unifying Z-Laplacian framework, whose instances can act as graph shift operators. As a generalization of the traditional graph Laplacian, the Z-Laplacian spans the space of all possible Z-matrices, i.e., real square matrices with nonpositive off-diagonal entries. We show that the Z-Laplacian can model general continuous-time dynamical processes, including information flows and epidemic spreading on a given graph. It is also closely related to general nonnegative graph filters in the discrete time domain. We showcase its flexibility by considering two applications. First, we consider a wireless communications networking problem modeled with a graph, where the framework can be applied to model the effects of the underlying communications protocol and traffic. Second, we examine a structural brain network from the perspective of low- to high-frequency connectivity.

I. INTRODUCTION

As a powerful representation for many complex systems, a network models entities and their interactions via vertices and edges. In the field of network science, studies of topological structures, including those of vertex centrality and community structure, have led to fundamental insights into the organization and function of social, biological, and technological systems [1]–[3]. To model dynamical properties on a given network, different dynamical processes can be defined over fixed topologies. Recent studies have demonstrated the fundamental interplay between dynamical operators and centrality and community structure measures [4]–[6].

In signal processing, we see the parallel development of graph signal processing (GSP). Starting with simple consensus problems on networks, Olfati-Saber, Fax, and Murray [7] developed methods that can be used to design and analyze distributed control of sensors, unmanned vehicles, and communications systems. Capable of dealing with directed networks, switching topologies, and time delays, their models are closely related to random walks on graphs. Sandryhaila and Moura [8] proposed a more general framework for defining linear invariant filters based on graph shift operators. By generalizing the classical discrete signal processing framework to graph topologies, well-developed theories and techniques can be extended to analyze more-complex problems involving interconnected systems and relational data sets [9].

By connecting these ideas from signal processing and network science, we investigate the mathematical duality between random walk and consensus processes on networks. We propose a class of discrete graph shift operators that are capable of modeling dynamical processes, including information flows and epidemic spreading. We demonstrate that, in this framework, these shifts span the space of all nonnegative matrices. We then adapt the discrete filters to continuous-time settings, introducing the *Z-Laplacian* with heterogeneous time delays. This theoretical generalization of the *parameterized Laplacian* framework [10] opens the door to signal processing analysis of continuous dynamical systems on networks.

The cross-disciplinary connection also allows us to apply the idea of dynamics modeling to signal processing problems. Under the parameterized Laplacian framework [10], we demonstrated that different parameterizations of random walk and consensus processes can lead to different perceived network structures on the same topology. In this paper, we make the following novel contributions:

- We propose the general continuous-time Z-Laplacian framework. The associated shifts span the space of *Z-matrices*, which are real square matrices with nonpositive off-diagonal entries [11]. The framework enables the modeling of epidemic and information diffusion (Theorems 1,2,4), unifying many existing linear operators in the literature.
- We connect discrete- and continuous-time dynamical processes to the GSP framework. In particular, we propose the *Z-Laplacian* operators as graph shifts, leading to induced signal processing techniques with corresponding dynamical process interpretations.

- We provide two signal processing examples of how different graph shift choices can lead to different conclusions in real applications.
  - For a wireless communications network with a fixed topology, we use the framework to model the traffic patterns under different communications protocols, coupling GSP with underlying protocol strategies and enabling the study of their interplay. This example illustrates how a dynamical process on a graph can be altered depending on the underlying assumptions about the traffic, communications rate, and protocol.
  - For structural brain networks, we use the framework to conduct frequency analysis from different dynamical perspectives, including information diffusion models made possible by the Z-Laplacian framework.

II. BACKGROUND

Classical discrete signal processing provides a wide range of tools to analyze data on regular structures, including filtering, transformation, compression, etc., GSP applies these tools to signals on graphs with arbitrary topologies [9].

Consider a directed graph $G = \{V, E, \boldsymbol{A}\}$, where $V = \{v_1, v_2, ..., v_N\}$ is the set of vertices, representing N elements in the system, and E is the set of edges that represent the pairwise interactions between the vertices. The topological structure of the system is captured by the weighted adjacency matrix $\boldsymbol{A}$. (Throughout, we will refer to weighted adjacency matrices simply as adjacency matrices.) The diagonal in- and out-degree matrices are respectively defined by $[\boldsymbol{D}_{\text{out}}]_{uu} = \sum_v \boldsymbol{A}_{uv}$ and $[\boldsymbol{D}_{\text{in}}]_{vv} = \sum_u \boldsymbol{A}_{uv}$, where $\boldsymbol{A}_{uv}$ is the (u, v) element of matrix $\boldsymbol{A}$. For undirected graphs, $\boldsymbol{D}_{\text{in}} = \boldsymbol{D}_{\text{out}} = \boldsymbol{D}$.

We define a *graph signal* $\theta : V \to \mathbb{R}$ as a mapping from V to the real numbers. We represent the graph signal at time step n (or t for continuous time) as a row vector $\boldsymbol{\theta}(n)$,[1] making the space of graphs signals identical to $\mathbb{R}^N$. A *graph filter* is a mapping from one graph signal to another,

$$\boldsymbol{\theta}(n + 1) = \boldsymbol{\theta}(n)\boldsymbol{H} \, , \tag{1}$$

where the filter is represented by an $N \times N$ matrix $\boldsymbol{H}$. Moreover, just like in classical signal processing, any linear shift-invariant filter can be expressed as

$$\boldsymbol{H} = \boldsymbol{H}(\boldsymbol{S}) = h_0\boldsymbol{I} + h_1\boldsymbol{S} + h_2\boldsymbol{S}^2 + ... + h_l\boldsymbol{S}^l \, , \tag{2}$$

where $\boldsymbol{S}$ is known as the graph shift operator corresponding to $\boldsymbol{H}$, the h_i, $0 \le i \le l$, are real coefficients, and l is the order of the filter. The graph shift operator $\boldsymbol{S}$ is not only the building block of shift-invariant filters, it is also closely related to the notions of frequency response, convolution, and Fourier transforms on graphs [12]. In [8], Sandryhaila and Moura derived a formal algebra based on $\boldsymbol{S}$, generalizing corresponding signal processing concepts to graph topologies.

There are at least two major definitions of the shift operator based on the graph adjacency matrix $\boldsymbol{A}$ or the (unnormalized) Laplacian matrix $\mathcal{L} = \boldsymbol{D} - \boldsymbol{A}$, and alternatives with other properties have also been proposed [13]. Because different shift operator definitions lead to divergent tools and algorithms, practitioners face difficult choices when applying GSP techniques. It is thus crucial to develop a basic understanding of how graph shift operators differ and relate to each other. For this purpose, we connect to the ideas from the parameterized Laplacian framework [10], where different operators can be interpreted as variants of random walk and consensus processes. We first reintroduce the framework in signal processing notation, described below and listed in Table I.

We start by representing a discrete-time random walk as a signal on a directed graph $G = \{V, E, \boldsymbol{A}\}$:

$$\boldsymbol{\theta}(n + 1) = \boldsymbol{\theta}(n)\boldsymbol{P} = \boldsymbol{\theta}(n)\boldsymbol{D}_{\text{out}}^{-1}\boldsymbol{A} \, . \tag{3}$$

Here the update filter $\boldsymbol{H} = \boldsymbol{P}$ is an $N \times N$ row (right) stochastic matrix. The graph signal $\boldsymbol{\theta}(n)$ represents the probability density of the random walk on each vertex at step n.

A consensus process on a graph can be viewed as the dual of a random walk, given by [10],

$$\boldsymbol{\theta}^{\text{CON}}(n + 1) = \boldsymbol{\theta}^{\text{CON}}(n)\boldsymbol{P}^{\text{CON}} = \boldsymbol{\theta}^{\text{CON}}(n)\boldsymbol{A}\boldsymbol{D}_{\text{in}}^{-1} \, . \tag{4}$$

Here, the filter $H = \boldsymbol{P}^{\text{CON}}$ is a column (left) stochastic matrix. Assuming $\boldsymbol{\theta}^{\text{CON}}(n = 0)$ is the initial signal, then at every time step each vertex updates its signal using the weighted average of its neighbors via multiplication by $\boldsymbol{P}^{\text{CON}}$. Unlike the graph signal in a random walk, entries in $\boldsymbol{\theta}^{\text{CON}}$ can be arbitrary (negative or positive) real numbers, without normalization constraints.

The parameterized Laplacian $\mathcal{L}$ can represent a continuous-time random walk, as in the differential equation

$$\frac{d\boldsymbol{\theta}(t)}{dt} = -\boldsymbol{\theta}(t)\mathcal{L} = -\boldsymbol{\theta}(t)\boldsymbol{T}^{-1}(\boldsymbol{I} - \boldsymbol{D}_{\boldsymbol{W}\text{out}}^{-1}\boldsymbol{W}) \, , \tag{5}$$

---

[1]In this paper, we adopt the Markov process convention, i.e., using row vertex signal vectors $\boldsymbol{\theta}(n)$ and right multiplying them by matrix operators, which contrasts with the algebraic convention we used in [6], [10]. We will also use $a_{uv} = [\boldsymbol{A}]_{uv}$ to represent entry (u, v) of a matrix $\boldsymbol{A}$ and $d_u = [\boldsymbol{D}]_{uu}$ to represent entry (u, u) of a diagonal matrix $\boldsymbol{D}$.

TABLE I: Glossary of terms and notation

Term	Description
Nonnegative matrix	A real matrix with all nonnegative entries
Z-matrix	A real matrix with all off-diagonal entries ≤ 0
$\boldsymbol{\theta}(t)$	Graph signal at continuous time t
$\boldsymbol{\theta}^{\mathrm{CON}}(t)$	Graph signal under consensus basis
$\boldsymbol{P}$	Random walk operator
$\boldsymbol{P}^{\mathrm{CON}}$	Consensus operator
$\boldsymbol{A}$	Adjacency matrix of graph G
$\boldsymbol{D}_{\mathrm{out}}$	Diagonal degree matrix of $\boldsymbol{A}$
$\boldsymbol{W}$	Transformed adjacency matrix of $\boldsymbol{A}$
$\boldsymbol{D}_{\boldsymbol{W}\,\mathrm{out}}$	Diagonal degree matrix of $\boldsymbol{W}$
$\boldsymbol{V_A}$	Diagonal matrix w/ dominating eigenvector of $\boldsymbol{A}$
$\boldsymbol{Z}$	Diagonal replicating factor matrix
$\boldsymbol{T}$	Diagonal delay factor matrix
$\mathcal{L}$	General Laplacian operator (examples follow)
Random walk Laplacian	$\boldsymbol{I} - \boldsymbol{D}_{\mathrm{out}}^{-1}\boldsymbol{A}$, given $\boldsymbol{A}$
Parameterized Laplacian	$\boldsymbol{T}^{-1}(\boldsymbol{I} - \boldsymbol{D}_{\boldsymbol{W}\,\mathrm{out}}^{-1}\boldsymbol{W})$, given $\boldsymbol{W} = \boldsymbol{AB}$
Replicator	Parameterized Laplacian with $\boldsymbol{W} = \boldsymbol{V_A}\boldsymbol{A}\boldsymbol{V_A}$
Z-Laplacian	$\boldsymbol{T}^{-1}(\boldsymbol{I} - \boldsymbol{Z}\boldsymbol{D}_{\mathrm{out}}^{-1}\boldsymbol{A})$, given $\boldsymbol{A}$

where $\boldsymbol{W} = \boldsymbol{AB}$ is a transformed adjacency matrix, $\boldsymbol{D}_{\boldsymbol{W}\,\mathrm{out}}$ is the diagonal matrix with $[\boldsymbol{D}_{\boldsymbol{W}\,\mathrm{out}}]_{uu} = \sum_v [\boldsymbol{W}]_{uv} = \sum_v [\boldsymbol{AB}]_{uv}$, and $\boldsymbol{B}$ and $\boldsymbol{T}$ are matrix parameters discussed below. We also use $\boldsymbol{W}$ to refer to the corresponding transformed graph itself, so that $\boldsymbol{D}_{\boldsymbol{W}\,\mathrm{out}}$ is the degree matrix of $\boldsymbol{W}$.

Compared with the random walk Laplacian $\mathcal{L} = \boldsymbol{I} - \boldsymbol{D}_{\mathrm{out}}^{-1}\boldsymbol{A}$, (5) has two additional parameter sets, $\boldsymbol{B}$ and $\boldsymbol{T}$. The diagonal matrix $\boldsymbol{B}$ consists of vertex bias factors that alter the random walk trajectory by giving neighbors additional weights. In a biased random walk, the transition probability from vertex u to v, denoted P_{uv}^{BRW}, is multiplied by a target bias factor b_v. In the parameterized Laplacian framework [10], [14], we introduced the idea of the *bias transformation* to relate the biased random walk to an unbiased version.

Lemma 1 (Bias transformation). *Any biased random walk on $G = (V, E, \boldsymbol{A})$, with the diagonal matrix $\boldsymbol{B}$ specifying vertex bias factors b_v, is equivalent to an unbiased random walk on the transformed graph $\boldsymbol{W} = \boldsymbol{AB}$. If G is undirected, then we instead consider the transformed graph $\boldsymbol{W} = \boldsymbol{BAB}$ to maintain edges having equal weight in both directions.*

Proof. See appendix. □

The other diagonal matrix parameter, $\boldsymbol{T}$, effects time delays for the continuous-time random walk,[2] providing inverse clock rates that control how long the walk stays at each vertex. (Without loss of generality, we constrain all the diagonal entries $\tau_u = [\boldsymbol{T}]_{uu} \geq 1$.) In Section IV, we will justify this intuition by connecting continuous-time processes to their discrete counterparts. Delayed continuous-time random walks can be captured using the *delay transformation*:

Lemma 2 (Delay transformation). *Any unbiased continuous-time random walk on $G = (V, E, \boldsymbol{A})$, with the diagonal matrix $\boldsymbol{T}$ specifying vertex delay factors τ_v, is equivalent to a continuous-time random walk with delay factors $\boldsymbol{I}$ on the transformed graph $\boldsymbol{W} = \boldsymbol{D}_{out}(\boldsymbol{T} - \boldsymbol{I}) + \boldsymbol{A}$, where $\boldsymbol{I}$ is the identity matrix.*

Proof. See appendix. □

Delay transformation enables us to view delay factors as self-loops, which can be absorbed into $\boldsymbol{W}$. A special case is when $\boldsymbol{T} = \alpha\boldsymbol{I}$ is a scalar matrix, which can be understood as rescaling the global clock rate, so that all delays are identical and equal to α.

Beyond the bias and delay transformations, the full parameterized Laplacian framework also has a similarity transformation that unifies the random walk and consensus processes on undirected graphs.

Lemma 3 (Similarity transformation). *Any continuous-time random walk on an undirected graph $G = (V, E, \boldsymbol{A})$ captured by the parameterized Laplacian $\mathcal{L} = \boldsymbol{T}^{-1}(\boldsymbol{I} - \boldsymbol{D}_{\boldsymbol{W}}^{-1}\boldsymbol{W})$, with the diagonal matrices $\boldsymbol{B}$ and $\boldsymbol{T}$ specifying vertex bias factors and vertex delay factors, is equivalent to a continuous-time dynamical process captured by the parameterized Laplacian $\mathcal{L} = (\boldsymbol{T}\boldsymbol{D_W})^{-1+\rho}(\boldsymbol{D_W} - \boldsymbol{W})(\boldsymbol{T}\boldsymbol{D_W})^{-\rho}$, up to a change of basis, where ρ is the basis parameter and $0 \leq \rho \leq 1$ (described below).*

---

[2]Bias transformation (also called "reweighing transformation" in [10]) applies to both discrete- and continuous-time dynamical processes [15].

Proof. See the "similarity transformation" in [10]. □

In particular, we recover the *random walk basis* by setting $\rho = 0$, and the *consensus basis* with $\rho = 1$. Another relevant case is the *symmetric basis* with $\rho = 0.5$, which leads to a Laplacian operator $\mathcal{L}^{\text{SYM}}$ represented by a symmetric matrix. In linear algebra, similarity is an equivalence relation for square matrices [11]. Similar matrices share many key properties, including their rank, determinant, and eigenvalues. Eigenvectors are also equivalent under a change of basis. For a given initial signal on an undirected graph with $T = I$ and $W = A$, the random walk (3) and consensus process (4) become identical at every time step, up to a change of basis. This follows from

$$
\begin{aligned}
D\mathcal{L}D^{-1} &= D(I - D^{-1}A)D^{-1} \\
&= I - AD^{-1} = I - P^{\text{CON}} = \mathcal{L}^{\text{CON}} ,
\end{aligned} \tag{6}
$$

where we used the fact that $A = A^T$ and $D_{\text{in}} = D_{\text{out}} = D$ for undirected graphs.

Using bias, delay, and similarity transformations, the parameterization Laplacian framework unifies various linear operators and their associated centrality and community structure measures from the network science literature [10]. In particular, here we introduce one special operator called the *replicator*, which is related to epidemic models.

Lemma 4 (Replicator operator)**.** *If $G = (V, E, A)$ is undirected and v_A is the eigenvector of the adjacency matrix A associated with the largest eigenvalue λ_{max}, so that $v_A A = \lambda_{max} v_A$, a biased random walk with the diagonal matrix $B = V_A$, whose bias factors are the components of v_A,[3] is defined by the stochastic matrix $P_W^{SYM} = \frac{1}{\lambda_{max}} A$ under the symmetric basis.*

Proof. By Lemma 1, the stochastic matrix of a biased random walk with $B = V_A$ is

$$
P_W = D_W^{-1} V_A A V_A ,
$$

where D_W is the diagonal degree matrix of the transformed graph $W = V_A A V_A$. Because $d_{W\,i} = \sum_j v_{A\,i} a_{ij} v_{A\,j} = v_{A\,i} \sum_j a_{ij} v_{A\,j} = \lambda_{\max} v_{A\,i}^2$, we have $D_W = \lambda_{\max} V_A^2$, and thus $P_W = \frac{1}{\lambda_{\max}} V_A^{-1} A V_A$. The continuous-time counterpart of P_W is represented by the random walk Laplacian $I - P_W$. By setting $\rho = -1/2$, $T = I$, and $D_W = \lambda_{\max} V_A^2$, according to Lemma 3 we have $\mathcal{L}_W^{\text{SYM}} = V_A(I - P_W)V_A^{-1} = I - \frac{1}{\lambda_{\max}} A$, therefore $P_W^{\text{SYM}} = \frac{1}{\lambda_{\max}} A$. □

In the sequel, we repeatedly use these transformations to design flexible operators that yield intuitive insight. While the similarity transformation becomes obsolete as we generalize to the Z-Laplacian, bias and delay transformations remain essential in practice for interpreting and comparing models on the same topology, as we will show in Sections V and VI.

Following the graph filter framework [8], we consider both P^{CON} and P as potential graph shift operators with interpretable dynamical parameters. Because both shifts and their continuous-time counterparts follow the aforementioned transformations, they form an infinite family of graph shifts on a given graph $G = (V, E, A)$. Note that these operators all have a dominating eigenvalue of 1, leading to an asymptotically stationary signal $\theta(n = \infty)$. During this process, the total signal (i.e., the sum of the components of $\theta(n)$) is always conserved under the random walk basis, preventing them from modeling non-conservative processes that grow or shrink over time.

III. EPIDEMIC MODEL AND NONNEGATIVE FILTERS

In this section, we will generalize the random walk and consensus processes to more-general operators, in the process unifying nonnegative linear graph filters. We begin by recalling a classic epidemic model, the susceptible-infected-susceptible (SIS) model.

A. Epidemic model on a graph

To generalize beyond conservative dynamical processes, we first redefine the classic SIS epidemic model on the graph $G = \{V, E, A\}$ [17] using graph signals. The graph signal $\theta^{\text{SIS}}(n)$ now represents the probabilities that each vertex is infected at step n, given by

$$
\begin{aligned}
\theta^{\text{SIS}}(n+1) &= \theta^{\text{SIS}}(n) H^{\text{SIS}} \\
&= \theta^{\text{SIS}}(n)(\mu A + (1 - \beta) I) .
\end{aligned} \tag{7}
$$

Here, each vertex has two states, susceptible or infected. When a vertex is *susceptible*, each of its neighbors will transition to the *infected* state with virus infecting probability μ. Once a vertex is *infected*, it will return to the *susceptible* state with virus curing probability β.

An important theorem about the SIS model is that its asymptotic behavior depends on the ratio μ/β, or the *effective transmissibility* of the virus. If the effective transmissibility is above the epidemic threshold, namely the inverse of the largest eigenvalue of the adjacency A, it will spread to a significant portion of the network. Otherwise, it will eventually die out.

---

[3]The replicator operator, not to be confused with a "replicating factor", also defines the maximum-entropy random walk under the random walk basis [16].

B. Epidemic model filters

To generalize (3), we introduce a uniform self-replicating factor z after each random walk step, resulting in the following update rule and corresponding difference equation:

$$[\boldsymbol{\theta}'(n+1)] = [\boldsymbol{\theta}'(n)]z\boldsymbol{P}$$
$$[\boldsymbol{\theta}'(n+1) - \boldsymbol{\theta}'(n)] = [\boldsymbol{\theta}'(n)](z\boldsymbol{P} - \boldsymbol{I}) . \tag{8}$$

Compared with $\boldsymbol{\theta}$, the signal vector $[\boldsymbol{\theta}']$ in (8) does not necessarily sum to 1, so it is more general and capable of modeling dynamical processes like information and epidemic spreading.

The difference equation in (8) provides intuition as to the corresponding dynamics. For the uniform self-replicating factor z, the corresponding growth rate is actually $(z - 1)$ for all vertices in the network. With $z = 1$, we have no replications and recover the conservative random walk process; with $z > 1$, we have an expanding process in which the incoming probability flow is scaled by z while the outgoing flow remains 1; and with $z < 1$, we have a shrinking process. Also note that in all cases z is the dominating eigenvalue of $z\boldsymbol{P}$, corresponding to the eigenvector $\mathbf{1}$, the all-ones vector. In practice we often restrict $z \geq 0$ so that the signal vector $[\boldsymbol{\theta}']$ always has a positive sum, which converges to 0 in shrinking processes.

For undirected graphs, we can rewrite (8) as

$$[\boldsymbol{\theta}'(n+1)]^{\text{SYM}} = [\boldsymbol{\theta}'(n)]^{\text{SYM}} \left(\frac{z}{\lambda_{\max}} \boldsymbol{A} \right)$$
$$= [\boldsymbol{\theta}'(n)]^{\text{SYM}} \left(\frac{z}{\lambda_{\max}} \boldsymbol{A}^0 + (1 - \beta)\boldsymbol{I} \right) , \tag{9}$$

where we have substituted in the replicator operator under the symmetric basis (see Lemma 4), with $[\boldsymbol{\theta}'(n+1)]^{\text{SYM}} = \boldsymbol{V_A} [\boldsymbol{\theta}'(n+1)] \boldsymbol{V_A}^{-1}$, and we have replaced $\boldsymbol{A} = \boldsymbol{A}^0 + \frac{\lambda_{\max}(1-\beta)}{z}\boldsymbol{I}$ to match the SIS epidemic model defined on adjacency matrix $\boldsymbol{A}^0$, as in (7). Here, the virus infecting probability from neighbors corresponds to $\frac{z}{\lambda_{\max}}$, and the virus curing probability at an infected vertex corresponds to β. Their ratio, the effective transmissibility, is $\frac{z}{\lambda_{\max}\beta}$, which determines how the epidemic will spread on the adjacency matrix $\boldsymbol{A}^0$.

With $0 \leq \beta \leq 1$, the inverse of the classic epidemic threshold, i.e., the dominating eigenvalue of $\boldsymbol{A}^0$, is $\frac{z+\beta-1}{z}\lambda_{\max}$. If the effective transmissibility $\frac{z}{\lambda_{\max}\beta}$ is greater than the threshold $\frac{z}{(z+\beta-1)\lambda_{\max}}$, or simply $z > 1$, we recover the definition of an expanding process. Similarly, conservative and shrinking processes are recovered with $z = 1$ and $z < 1$, respectively.

If we apply the duality between the random walk and consensus models to the non-conservative process in (8), we have

$$[\boldsymbol{\theta}'(n+1)] = [\boldsymbol{\theta}'(n)]z\boldsymbol{D}_{\text{out}}^{-1}\boldsymbol{A}$$
$$[\boldsymbol{\theta}'(n+1)]^{\text{CON}} = [\boldsymbol{\theta}'(n)]^{\text{CON}}z\boldsymbol{A}\boldsymbol{D}_{\text{in}}^{-1} . \tag{10}$$

Here, the dual is a graph filter where each vertex first updates its signal using the weighted neighbor average and then the average signal is amplified by a factor z, leading to $[\boldsymbol{\theta}'(n=\infty)]^{\text{CON}} = \mathbf{0}$ with $z < 1$ or $[\boldsymbol{\theta}'(n=\infty)]^{\text{CON}} = \infty$ with $z > 1$.

C. General nonnegative graph filters

To further generalize beyond epidemics with uniform self-replications, consider the following update and difference equations:

$$[\boldsymbol{\theta}(n+1)] = [\boldsymbol{\theta}(n)]\boldsymbol{Z}\boldsymbol{P}$$
$$[\boldsymbol{\theta}(n+1) - \boldsymbol{\theta}(n)] = [\boldsymbol{\theta}(n)](\boldsymbol{Z}\boldsymbol{P} - \boldsymbol{I}) , \tag{11}$$

where we have used a positive diagonal matrix $\boldsymbol{Z}$,[4] whose diagonal elements $[\boldsymbol{Z}]_{vv}$ model a shrinking or expanding *replicating factor* for each vertex v. The random walk step is now followed by a vertex specific replicating process, with a generally non-uniform replicating factor specified by $\boldsymbol{Z}$.

Applying the same duality between consensus and random walk processes to this more general dynamical process, we have

$$[\boldsymbol{\theta}(n+1)] = [\boldsymbol{\theta}(n)]\boldsymbol{Z}\boldsymbol{D}_{\text{out}}^{-1}\boldsymbol{A}$$
$$[\boldsymbol{\theta}(n+1)]^{\text{CON}} = [\boldsymbol{\theta}(n)]^{\text{CON}}\boldsymbol{A}\boldsymbol{D}_{\text{in}}^{-1}\boldsymbol{Z} . \tag{12}$$

To interpret the operator $\boldsymbol{A}\boldsymbol{D}_{\text{in}}^{-1}\boldsymbol{Z}$, we focus on the dynamics of a specific vertex u, given by

$$[\boldsymbol{\theta}(n+1)]_u^{\text{CON}} = \sum_v [\boldsymbol{\theta}(n)]_v^{\text{CON}}[\boldsymbol{A}]_{vu}[\boldsymbol{D}_{\text{in}}]_u^{-1}[\boldsymbol{Z}]_{uu} , \tag{13}$$

---

[4]The replicating factors play the same role in the continuous-time Z-Laplacian, thus the notation $\boldsymbol{Z}$ here.

where $[\boldsymbol{A}]_{vu}[\boldsymbol{D}_{\text{in}}]_u^{-1}$ forms a weighted probability distribution over all incoming neighbors of u. Notice that the replicating factor of the incoming signals $[\boldsymbol{Z}]_{uu}$ only depends on the target vertex u. Compared with the uniform replicating factor z in (10), the order of matrix multiplication by $\boldsymbol{Z}$ now matters. Under the consensus model, with vertex u averaging the signals of neighbors v, all signals are multiplied by the same factor of $[\boldsymbol{Z}]_{uu}$, whereas this factor is v dependent under the random walk basis.

Unlike the less general filters we have discussed previously, both operators in (12) span the same vector space. This equivalence is easiest to show if we have an undirected graph and let[5] $\boldsymbol{Z} = \boldsymbol{D}$, leading to

$$\boldsymbol{A}\boldsymbol{D}_{\text{in}}^{-1}\boldsymbol{Z} = \boldsymbol{A}\boldsymbol{D}^{-1}\boldsymbol{D} = \boldsymbol{D}\boldsymbol{D}^{-1}\boldsymbol{A} = \boldsymbol{Z}\boldsymbol{D}_{\text{out}}^{-1}\boldsymbol{A} \,, \tag{14}$$

where we used $\boldsymbol{A} = \boldsymbol{A}^T$ and $\boldsymbol{D} = \boldsymbol{D}_{\text{in}} = \boldsymbol{D}_{\text{out}}$.

In fact, for general directed graphs, the vector space spanned by both operators contains all possible nonnegative matrices, and we call them *general nonnegative filters*. To prepare for this theoretical unification, we first consider the following lemma regarding the adjacency matrix and random walks.

Lemma 5 (Adjacency mapping). *For every directed weighted graph $G = \{V, E, \boldsymbol{A}\}$, there is a unique transition matrix, $\boldsymbol{P_A} = \boldsymbol{D}_{out}^{-1}\boldsymbol{A}$, that captures an unbiased random walk on $\boldsymbol{A}$. Conversely, given a stochastic matrix $\boldsymbol{P}$, there is an infinite family of adjacency matrices $\mathcal{A}_{\boldsymbol{P}}$ whose random walk process is consistent with $\boldsymbol{P}$, denoted as*

$$\mathcal{A}_{\boldsymbol{P}} = \{\boldsymbol{\Gamma}\boldsymbol{P} : \boldsymbol{\Gamma} \text{ is a positive diagonal matrix.}\}$$

Proof. Since $\boldsymbol{D}_{\text{out}}$ is uniquely determined by a given $\boldsymbol{A}$, then every directed network uniquely defines a random walk process. However, given a transition matrix $\boldsymbol{P}$, there remains N degrees of freedom to specify the underlying network. Intuitively, the degrees of freedom can be interpreted as row scalings that proportionally multiply all outgoing edges of a vertex, thus preserving the random walk distribution leaving from the given vertex. Here we represent these degrees of freedom using the entries of $\boldsymbol{\Gamma}$. $\qquad\square$

Now we are ready to prove the unification theorem for nonnegative filters expressed with an arbitrary basis.

Theorem 1 (Basis Unification). *For any general nonnegative filter defined as $\boldsymbol{Z}\boldsymbol{D}_{out}^{-1}\boldsymbol{A}$ on graph $G = \{V, E, \boldsymbol{A}\}$, there is an equivalent dual filter defined as $(\boldsymbol{D}'^{-1}\boldsymbol{Z}')^{1-\rho}\boldsymbol{A}'(\boldsymbol{D}'^{-1}\boldsymbol{Z}')^{\rho}$ on a dual graph $\boldsymbol{A}' \in \mathcal{A}_{\boldsymbol{P}}$, under any given basis parameter $0 \le \rho \le 1$.*

Proof. Assume we have two equivalent filters defined on two different graphs $\boldsymbol{A}$ and $\boldsymbol{A}'$. Then

$$\boldsymbol{Z}\boldsymbol{D}_{\text{out}}^{-1}\boldsymbol{A} = (\boldsymbol{D}'^{-1}\boldsymbol{Z}')^{1-\rho}\boldsymbol{A}'(\boldsymbol{D}'^{-1}\boldsymbol{Z}')^{\rho}$$
$$\boldsymbol{A}' = (\boldsymbol{D}'^{-1}\boldsymbol{Z}')^{\rho}\boldsymbol{Z}\boldsymbol{P_A}(\boldsymbol{D}'^{-1}\boldsymbol{Z}')^{-\rho} \,. \tag{15}$$

Setting $\boldsymbol{Z}' = \boldsymbol{D}'$, we have $\boldsymbol{A}' = \boldsymbol{Z}\boldsymbol{P_A}$. Applying Lemma 5, the dual graph $\boldsymbol{A}'$ is a row scaled version of $\boldsymbol{A}$ by setting $\boldsymbol{\Gamma} = \boldsymbol{Z}$. $\qquad\square$

By Theorem 1, the duality in (12) essentially leads to another filter on a different graph. When $\rho = 1$ and $\boldsymbol{D}' = \boldsymbol{D}_{\boldsymbol{A}'\text{in}}$, we have the equivalence between the consensus and random walk processes. As a result, we will no longer need to separately specify dynamical processes in random walk, consensus, or any other basis. We will thus suppress the superscript notations on filters and signals in the following sections.

Next, we prove that general nonnegative filters span all possible nonnegative matrices:

Theorem 2 (Generality Theorem). *Given an arbitrary nonnegative matrix $\boldsymbol{H}$, we can associate it with a general nonnegative filter $\boldsymbol{H} = \boldsymbol{Z}\boldsymbol{D}_{out}^{-1}\boldsymbol{A}$, which models a general dynamical process on a graph $G = \{V, E, \boldsymbol{A}\}$.*

Proof. Let $\boldsymbol{A} = \boldsymbol{H}$. For any nonnegative matrix $\boldsymbol{H}$, $\boldsymbol{A} = \boldsymbol{H}$ represents a graph adjacency matrix. By setting $\boldsymbol{Z} = \boldsymbol{D}_{\text{out}}$, we have $\boldsymbol{H} = \boldsymbol{Z}\boldsymbol{D}_{\text{out}}^{-1}\boldsymbol{A}$. $\qquad\square$

The simple proof essentially states that any nonnegative matrix can be interpreted as an epidemic model based on a random walk with non-uniform replicating factors that are proportional to the vertex degrees. From a degrees-of-freedom perspective, the non-uniform replicating factor $\boldsymbol{Z}$ perfectly matches the row normalization constraint.

Combining Theorems 1 and 2, we observe the full generality of the proposed nonnegative graph filters. Based on the algebraic framework introduced in [8], these nonnegative shift operators also define a shift-invariant vector space, which can be generally expressed as $\mathcal{F} = \left\{\boldsymbol{K} : \boldsymbol{K} = \sum_{l=0}^{N} h_l\boldsymbol{H}^l \mid h_l \in \mathbb{R}\right\}$. This unification opens the door to discrete signal processing methodologies while connecting the concepts of random walk, epidemics, and information diffusion on networks.

---

[5]Mathematically, one has the liberty to manipulate the parameters in $\boldsymbol{Z}$ and $\boldsymbol{T}$. In practice, however, we suggest setting them based on domain knowledge for intuition and interpretation.

IV. CONTINUOUS-TIME FILTERS AND Z-LAPLACIAN

Based on the discrete nonnegative graph filters in (11), we can define continuous dynamical processes by replacing the difference equations with differential equations, yielding[6]

$$\frac{d\boldsymbol{\theta}(t)}{dt} = -\boldsymbol{\theta}(t)\boldsymbol{\mathcal{L}} = -\boldsymbol{\theta}(t)\boldsymbol{T}^{-1}(\boldsymbol{I} - \boldsymbol{Z}\boldsymbol{D}_{\text{out}}^{-1}\boldsymbol{A}) \ , \tag{16}$$

where we define the operator $\boldsymbol{T}^{-1}(\boldsymbol{I} - \boldsymbol{Z}\boldsymbol{D}_{\text{out}}^{-1}\boldsymbol{A})$ as the *Z-Laplacian*.

Here the positive diagonal matrix $\boldsymbol{T}$ represents the time delay, or inverse clock rate, at each vertex. When $\boldsymbol{Z} = \boldsymbol{I}$, we have $\boldsymbol{\mathcal{L}} = \boldsymbol{T}^{-1}(\boldsymbol{I} - \boldsymbol{P})$, which corresponds to a special case of the parameterized Laplacian we introduced in [6]. Compared with discrete-time filters with uniform time steps, (16) allows asynchronous updates by modeling the movement of random walks as Poisson processes for which the waiting times between jumps are exponentially distributed with mean parameters specified by $\boldsymbol{T}$ [15].

To connect the continuous-time Z-Laplacian to discrete filters, we first prove the following Lemma over a short time interval δ.

Lemma 6 (Discrete approximation). *Given the graph signal $\boldsymbol{\theta}(t)$ and the continuous-time Z-Laplacian $\boldsymbol{T}^{-1}(\boldsymbol{I} - \boldsymbol{Z}\boldsymbol{D}_{\text{out}}^{-1}\boldsymbol{A})$, the graph signal at time $t + \delta$ can be approximated as $\delta \to 0$ by*

$$\lim_{\delta \to 0} \boldsymbol{\theta}(t + \delta) = \boldsymbol{\theta}(t)e^{-\boldsymbol{\mathcal{L}}\delta} = \boldsymbol{\theta}(t)(\boldsymbol{I} - \lim_{\delta \to 0} \delta\boldsymbol{\mathcal{L}}) \ ,$$

where $\boldsymbol{I} - \delta\boldsymbol{\mathcal{L}}$ represents a discrete time filter.

Proof. See appendix. $\square$

Letting $\delta = \frac{1}{\lambda}$, we rewrite the discrete time filter as

$$\boldsymbol{\Phi} = \boldsymbol{I} - \frac{1}{\lambda}\boldsymbol{\mathcal{L}} = \boldsymbol{I} - \frac{1}{\lambda}\boldsymbol{T}^{-1}(\boldsymbol{I} - \boldsymbol{Z}\boldsymbol{D}_{\text{out}}^{-1}\boldsymbol{A}) \ . \tag{17}$$

Substituting $\boldsymbol{\mathcal{L}} = \lambda(\boldsymbol{I} - \boldsymbol{\Phi})$, we can write the solution of (16) as

$$\boldsymbol{\theta}(t) = \boldsymbol{\theta}(0)e^{-\boldsymbol{\mathcal{L}}t} = \boldsymbol{\theta}(0)e^{-(\boldsymbol{I}-\boldsymbol{\Phi})\lambda t} = \boldsymbol{\theta}(0)e^{-\lambda t}e^{\lambda\boldsymbol{\Phi}t} \ . \tag{18}$$

Using the "uniformization technique" [18] we can write matrix exponentiation in terms of an infinite sum of matrix powers to obtain

$$\boldsymbol{\theta}(t) = \boldsymbol{\theta}(0)e^{-\lambda t}\sum_{k=0}^{\infty}\frac{1}{k!}(\lambda\boldsymbol{\Phi}t)^k = \boldsymbol{\theta}(0)\sum_{k=0}^{\infty}\frac{e^{-\lambda t}}{k!}(\lambda\boldsymbol{\Phi}t)^k$$

$$= \boldsymbol{\theta}(0)\sum_{k=0}^{\infty}P_{\text{Poi}}(k,t)\boldsymbol{\Phi}^k \ , \tag{19}$$

where $P_{\text{Poi}}(k,t)$ represents a Poisson probability mass function of a discrete-time random walk with intensity λ taking k steps during the time interval $[0, t)$.

As (19) demonstrates, the continuous process can be interpreted as a weighted infinite sum of powers of $\boldsymbol{\Phi}$, representing discrete time random walks of different lengths. The following theorem give us intuition for the delay factors $\boldsymbol{T}$.

Theorem 3 (Delay interpretation). *Given the continuous-time Z-Laplacian $\boldsymbol{T}^{-1}(\boldsymbol{I} - \boldsymbol{Z}\boldsymbol{D}_{\text{out}}^{-1}\boldsymbol{A})$ and its discrete time approximation $\boldsymbol{\Phi}$, the delay factor $[\boldsymbol{T}]_{uu}$ of vertex u is proportional to the expected "waiting steps" on vertex u for the approximated discrete-time random walk.*

Proof. See appendix. $\square$

Lemma 6 and Theorem 3 provide interpretation of the delay factors in $\boldsymbol{T}$ and connect the continuous- and discrete-time models. In the next section we give an example, applying the continuous-time model to a communications network.

Next, we prove the central theorem of the Z-Laplacian framework, which extends the generality Theorem (Theorem 2) to the continuous domain.

Theorem 4 (Continuous-Time Generality Theorem). *For an arbitrary Z-matrix $\boldsymbol{\mathcal{L}}$, we can associate it with a Z-Laplacian $\boldsymbol{\mathcal{L}} = \boldsymbol{T}^{-1}(\boldsymbol{I} - \boldsymbol{Z}\boldsymbol{D}_{out}^{-1}\boldsymbol{A})$, which models a general continuous-time dynamical process on a graph (with self-loops) $G = \{V, E, \boldsymbol{A}\}$.*

---

[6]The variable t is a real number representing continuous time.

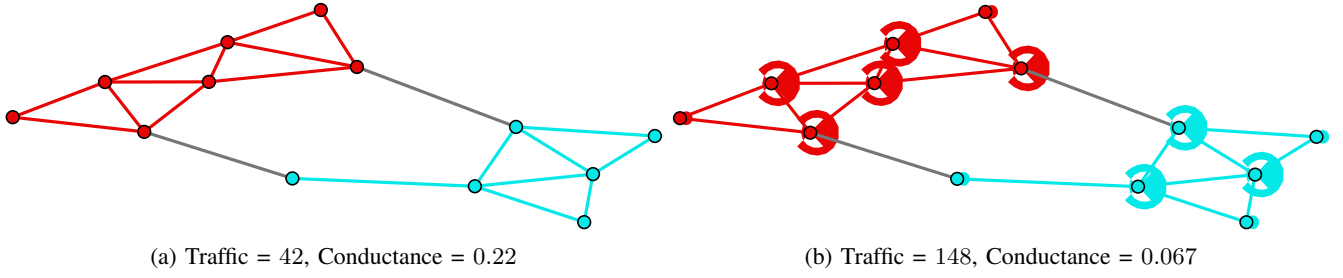(a) Traffic = 42, Conductance = 0.22   (b) Traffic = 148, Conductance = 0.067

Fig. 1: Communications network example graph (see text). Colors indicate graph subset membership after bottleneck discovery. (a) An ideal network graph with uniform and orthogonal connectivity and no delays. (b) To model a random access MAC protocol, self-loops are introduced to model traffic delay, indicated graphically as colored circles around the vertices, the size of the circles being proportional to delay. In both subfigures, the primary communications bottleneck lies at the boundary of the two vertex communities, indicated by their different colors. The total traffic is measured by the total weighted degree, and the global efficiency is measured by the conductance.

Proof. Without loss of generality, we set $\boldsymbol{T} = \delta \boldsymbol{I}$, and thus

$$-\boldsymbol{\mathcal{L}} = \frac{1}{\delta}(\boldsymbol{Z}\boldsymbol{D}_{\text{out}}^{-1}\boldsymbol{A} - \boldsymbol{I})$$
$$\boldsymbol{Z}\boldsymbol{D}_{\text{out}}^{-1}\boldsymbol{A} = \boldsymbol{I} - \delta\boldsymbol{\mathcal{L}} \ . \tag{20}$$

Let $\boldsymbol{\mathcal{L}}$ be an arbitrary Z-matrix, i.e., a real square matrix with nonpositive off-diagonal entries [11]. Then $-\boldsymbol{\mathcal{L}}$ has only nonnegative off-diagonal entries. If there are negative diagonal entries, we set $0 \leq \delta \leq 1/\max_i |[\boldsymbol{\mathcal{L}}]_{ii}|$, making $\boldsymbol{I} - \delta\boldsymbol{\mathcal{L}}$ a nonnegative matrix.

By setting $\boldsymbol{Z} = \boldsymbol{D}_{\text{out}}$, we have $\boldsymbol{A} = \boldsymbol{I} - \delta\boldsymbol{\mathcal{L}}$, which represents a graph adjacency matrix given any Z-matrix $\boldsymbol{\mathcal{L}}$. □

Theorem 4 justifies the generalized continuous-time operator as the Z-Laplacian, which is a unifying framework for all potential shift operators. The Z-Laplacian is closely related to the *generalized Laplacian* [19], [20], with the latter being the symmetric subset of the Z-Laplacian.

V. COMMUNICATIONS NETWORK ANALYSIS

It is common practice to use a graph to model a communications network, with edges modeling one-hop connectivity between nodes. For example, convergence analysis of a consensus process as in (4) is linked with the properties of the adjacency matrix of the graph [7]. This assumes an underlying communications protocol based on the connectivity, where each iteration requires every node to have a message exchange with its one-hop neighbors. This is a useful abstraction, but does not model the impact of channel variation, rate, multi-user interference, or delay, as occur in wireless communications applications such as sensor and mobile ad-hoc networks. Employing the Z-Laplacian framework enables the modeling of delays and multi-user collisions, which are a function of the communications protocol and the graph topology. To illustrate this, we consider analysis of a communications network to include delay effects and their linkage with the topology and the medium access control (MAC) protocol. We study the isolation of network bottlenecks, including the impact of MAC choices, as well as topology alteration by inserting nodes and changing bandwidth allocation to improve network connectivity.

A. Networking Bottlenecks and the Z-Laplacian

Given a network graph, consider the problem of identifying bottlenecks where traffic may funnel through a small subset of nodes and create excess delays in the overall network performance. We build on prior work for bottleneck identification based solely on the network topology [21], [22], briefly reviewed next. We use a running example throughout this section, illustrated in Figures 1, 2, and 3. In the figures, colors indicate graph subset membership, colored disks around each vertex indicate self-loops whose weight is proportional to communications delay at that vertex (with larger area implying more delay), and graphical edge thickness is proportional to link rate between the two vertices (with a thicker edge implying higher bandwidth).

In the simplest setting [21], [22], we assume that all communications are orthogonal, with no multi-user interference or additional delay, and that each vertex always has a packet to transmit (a fully saturated network traffic model). Recalling our notation from Section II, the network graph is $G = \{V, E, \boldsymbol{A}\}$, and elements of $\boldsymbol{A}$ are denoted a_{ij}. We begin with the graph network model shown in Fig. 1. Assuming each undirected edge carries one unit of traffic in both directions, the overall network traffic equals the total weighted degree, or $2 \times |E| = 42$ for our example. Under the Z-Laplacian framework, as in

(16), this simple traffic pattern can be captured by setting both the vertex delays and replicating factors to the identity matrix, so $\boldsymbol{Z} = \boldsymbol{T} = \boldsymbol{I}$ and

$$\mathcal{L} = \boldsymbol{I} - \boldsymbol{D}^{-1}\boldsymbol{A} \, , \tag{21}$$

where $\boldsymbol{D}$ is the (diagonal) degree matrix (see Table I). This corresponds to the idealized case in Fig. 1(a). By setting $\boldsymbol{T} = \boldsymbol{I}$, we assume each vertex spends one unit of delay to process the packet, whereas additional delays will represent interference or collisions, as described below. Here we assume that packets only flow along graph edges and that each packet is only sent once (there is no duplication or broadcasting of packets), as indicated by $\boldsymbol{Z} = \boldsymbol{I}$.

To find and quantify the primary network bottleneck under different MAC protocols, we use the more flexible transformed graph $\boldsymbol{W}$ for definitions (see Table I). For the base-case Laplacian in (21), we simply set $\boldsymbol{W} = \boldsymbol{A}$.

We split the vertices into two subsets, $S \subseteq V$ and its complement $\bar{S} = V \setminus S$. Let $\text{cut}(S, \bar{S}) = \sum_{i \in S, j \in \bar{S}}(w_{ij} + w_{ji})$ denote the total weights of all edges between S and $\bar{S}$. Let $\text{vol}(S) = \sum_{i \in S} d_i = \sum_{i \in S, j \in V} w_{ij}$ denote the total (undirected, weighted) degree over all vertices in S. The ratio of these two quantities measures the balanced separation strength of the transformed graph, given by

$$\phi(S) = \frac{\text{cut}_{\boldsymbol{W}}(S, \bar{S})}{\min\left\{\text{vol}(S), \text{vol}(\bar{S})\right\}} \, . \tag{22}$$

The quantity $\phi(S)$ is called the *conductance*, and we will use its minimum

$$\phi^*(G) = \min_{S \in V} \phi(S) = \phi(S^*) \tag{23}$$

to measure the network bottleneck and its minimizer S^* to locate the bottleneck at its boundary[7]. The base-case Laplacian leads to a minimum conductance of 0.078.

B. MAC Protocols and the Z-Laplacian

The baseline analysis above assumes ideal and orthogonal communications, without any consideration of delay. Next, we adjust parameters of the Z-Laplacian to model different dynamical processes (protocols) on the same topology. Note that each protocol will induce a potentially different primary bottleneck position and strength according to (23), without changing the topology.

Generally, depending on the protocol and topology, the vertex delays will be non-uniform. Consider a random access MAC, which will result in transmission collisions and packet delays due to the need for backoff and retransmission. As one modeling approach, let the vertex delays be proportional to the vertex degree, implying that higher-degree vertices will have more communications delay because collisions are more likely. Specifically, let $\boldsymbol{T} = \boldsymbol{D}$ so the delays are equal to the degree for each vertex.[8] The resulting Z-Laplacian is

$$\mathcal{L} = \boldsymbol{D}^{-1}(\boldsymbol{I} - \boldsymbol{D}^{-1}\boldsymbol{A}) \, . \tag{24}$$

By appealing to the delay transformation in Lemma 2, delays are modeled by introducing vertex self-loops, and we have the corresponding transformed graph $\boldsymbol{W} = \boldsymbol{D}(\boldsymbol{T} - \boldsymbol{I}) + \boldsymbol{A}$. Applying this transformation to our example, again assuming a saturated traffic model, we obtain Fig. 1(b). Now the more realistically modeled network is considerably less efficient than its idealized version, with total traffic $2 \times |E| = 148$ and a minimum conductance of 0.067. Here, we have repeated the above bottleneck discovery algorithm, with the two resulting subsets shown in Fig. 1(b). Although not evident from this example, we emphasize that changing the network protocol may result in a different bottleneck position and strength.

Suppose now that we employ a time-division multiple access (TDMA) protocol to minimize collisions and enhance overall network throughput. Fig. 2(a) models this case as a graph filter, where each vertex evenly divides its transmission time among its neighbors. As a result, edges between high-degree vertices have a reduced effective bandwidth due to their smaller share of the time-division allocation. This is readily captured under the Z-Laplacian framework using the bias transformation (Lemma 1):

$$\mathcal{L} = \boldsymbol{T}^{-1}[\boldsymbol{I} - \boldsymbol{D}_{\boldsymbol{W}}^{-1}(\boldsymbol{D}^{-1}\boldsymbol{A}\boldsymbol{D}^{-1})] \, , \tag{25}$$

where we have applied the undirected version of the bias transformation on both sides of $\boldsymbol{A}$ and $\boldsymbol{D}_{\boldsymbol{W}'}^{-1}$ is the diagonal degree matrix of the transformed graph $\boldsymbol{W}' = \boldsymbol{D}^{-1}\boldsymbol{A}\boldsymbol{D}^{-1}$. For comparison, we started with the same traffic as in Fig. 1(a), with each edge carrying one unit of traffic in both directions. We first saturated the time-divided effective bandwidth and then visualized the remaining traffic as self-loops or, effectively, vertex delay factors $\boldsymbol{T}$. The resulting transformed graph is $\boldsymbol{W} = \boldsymbol{D}_{\boldsymbol{W}'}(\boldsymbol{T} - \boldsymbol{I}) + \boldsymbol{W}'$, as visualized in Fig. 2(a). It is a more efficient system compared to that of Fig. 1(b), with increased minimum conductance (now equal to 0.078) and no redundant traffic (equal to 42).

---

[7]We use the optimization algorithm introduced in [10] to find both.
[8]More complicated super-linear scaling can be implemented by other choices for the delay factors.

(a) Traffic = 42, Conductance = 0.078
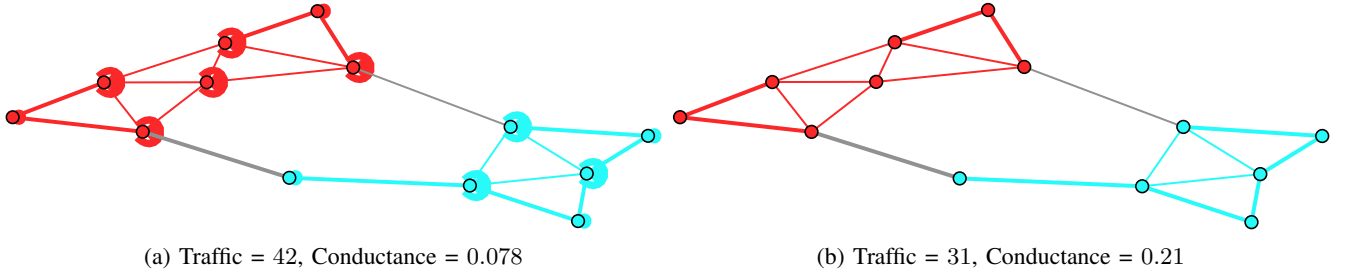
(b) Traffic = 31, Conductance = 0.21

Fig. 2: Communications network example, continued (see text). (a) A TDMA protocol is modeled with self-loops modeling the delay time at each vertex due to time slot allocation, assuming a saturated traffic load. (b) The same TDMA protocol is modeled, now with the traffic load perfectly matched to the available time slots, resulting in no delays.
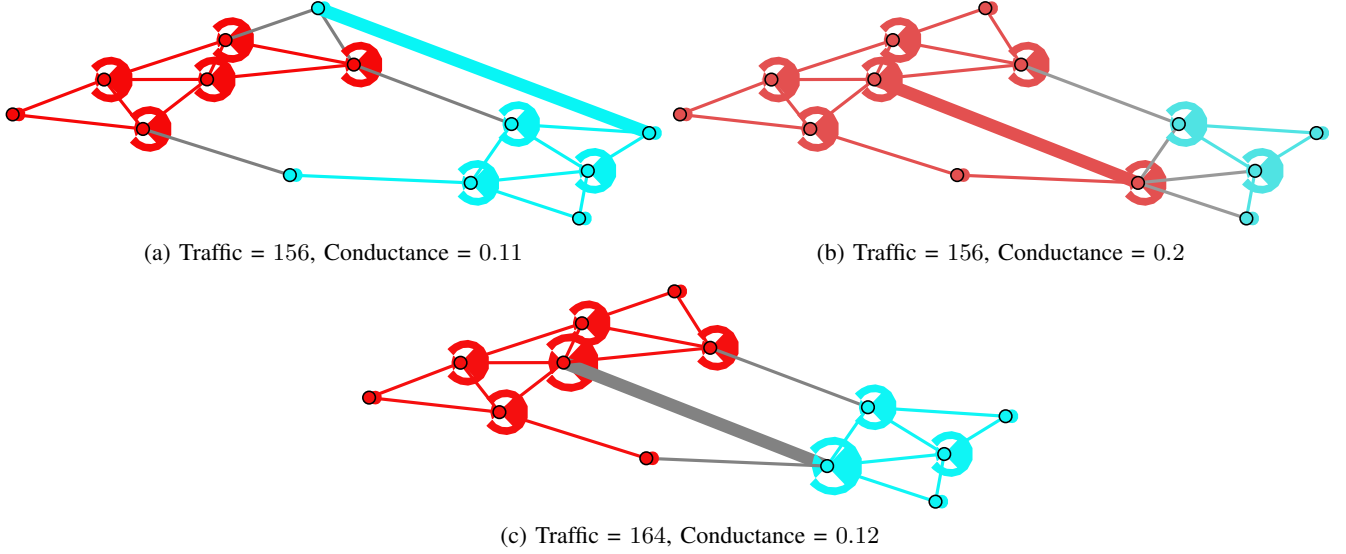

(a) Traffic = 156, Conductance = 0.11

(b) Traffic = 156, Conductance = 0.2

(c) Traffic = 164, Conductance = 0.12

Fig. 3: Communications network example, continued (see text). Two examples of bottleneck alleviation, using the results from Fig. 1(b), by introducing a new edge, shown as the thick blue line in (a) and the thick red line in (b). While the total traffic measure is the same for both cases, (b) has higher conductance and leads to a more globally efficient network. In (c), we include the additional delays caused by the introduction of the new edge.

When the network traffic load becomes lighter, TDMA protocols are less efficient in terms of utilizing the full bandwidth. Fig. 2(b) models a perfectly loaded TDMA system, where the traffic is precisely matched to the capacity of each edge and each message hits its time slot without any delay. Compared with the perfectly loaded random access system in Fig. 1(a), the network carries much less total traffic. These examples illustrate how the traffic load and protocol-induced delays can be modeled together to study the overall network performance, including the discovery of bottlenecks.

C. Healing Networks by Vertex Insertion and Bandwidth Allocation

Once a bottleneck has been identified, we can consider network healing by augmenting the network. There are various ways to do this, such as bandwidth reallocation to reduce delays. Here, we consider augmenting the network topology by introducing a (perhaps higher bandwidth) link across the bottleneck. We limit our study to the introduction of a new edge in the existing graph, although the general framework allows for more elaborate combinations of new vertex introduction and optimized resource allocation, which can correspond to an adaptive enhancement at the network physical layer and/or the MAC. There are many possibilities, and this is an interesting topic for future study.

We continue our running example in this section, beginning with the random access protocol model in Fig. 1(b). Figs. 3(a) and 3(b) depict two cases where a new edge is introduced. The new edges have a bandwidth that is four times greater than the preexisting edges (and are hence graphically thicker). We further assume the new edges do not introduce new interference to the preexisting edges, and so no new delays are incurred. The first case, shown in Fig. 3(a), connects two peripheral vertices at the corners of the two subsets, whereas the second case, shown in Fig. 3(b), connects two central vertices on opposite sides of the bottleneck.
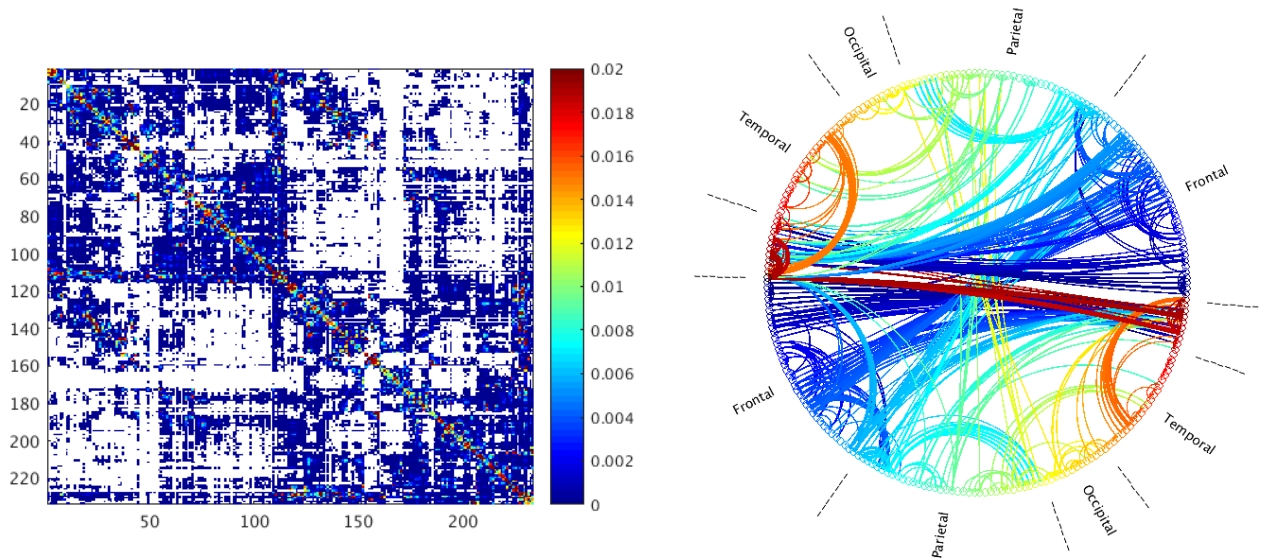
Fig. 4: The adjacency matrix and 2% visualization of the average structural brain network

In line with our intuition, the cross-link between central vertices in Fig. 3(b) leads to an overall more efficient system as measured by conductance. The central vertices are more available to the entire network on both sides of the bottleneck. For both cases we also repeated the bottleneck discovery after the new edge was introduced, as shown in Fig. 3 with the new color groupings. Comparing with Fig. 1(b), the new edge in Fig. 3(a) has less of an impact on the bottleneck subsets than the more effective new edge in Fig. 3(b).

To demonstrate that changing the network protocol on the same topology may result in different bottlenecks, we also repeated the bottleneck discovery with the assumption that the new edge does introduce delays proportional to the increased vertex degrees. As shown in Fig. 3(c), the additional delays naturally lead to a less efficient system. Compared with Fig. 1(b), the bottleneck location remains the same with the added edge but now with lower minimum conductance.

This analysis can be expanded to discover bottlenecks and the corresponding optimal choices for new edges in an iterative manner, providing network enhancement options and adding robustness.

VI. EXPLORING GRAPH FREQUENCY ANALYSIS FOR BRAIN CONNECTIVITY

To illustrate how the Z-Laplacian based graph filters can be used in frequency analysis, we consider structural brain networks built from diffusion weighted imaging MRI scans[9] of 40 experiment participants [23]. Frequency-specific brain activity is well known and associated with different brain states. Graph frequency analysis is thus a useful signal processing tool for studying functional brain networks [24], [25]. Recently, there is also evidence that structural brain networks may also organize by graph spectrum [26]–[28]. However, previous work is mostly limited to the standard shift operators based on graph adjacency A or (unnormalized) Laplacian matrices $\mathcal{L} = D - A$. Here we demonstrate the flexibility of the Z-Laplacian in graph frequency analysis of given structural networks. In the future, we plan to investigate direct signal analysis of functional networks.

To demonstrate frequency analysis based on different candidate shift operators, we construct multiple Z-Laplacian operators using the same average network over all 40 samples. Fig. 4 depicts the undirected weighted adjacency structure of the average structural network and a corresponding 2% visualization.[10] The visualization uses a circular layout similar to a connectogram [29]. We have also labeled the four major regions of the cerebral cortex in the human brain, namely frontal lobe, parietal lobe, occipital lobe, and temporal lobe. For a better cross-hemisphere visualization, we adopted the circular symmetry and concatenated left and right hemispheres head to tail. We color coded the brain regions from blue to red in each hemisphere, and the stem is colored black. There are other brain regions in the network that are not labeled (dark red). Some vertices from the limbic lobe are merged into the frontal (blue) and parietal (green) lobes. Notice here the averaged network is quite dense with 27,540 total non-zero edges from all 40 samples.

---

[9]Diffusion weighted imaging captures bundles of white matter fibers, revealing the anatomical connections between different parts of the brain.

[10]An $x\%$ visualization displays the $x\%$ of edges with the greatest weight. The percentile measure includes zero-weight edges or non-edges. In Fig. 4, the 2% visualization contain the top 1,096 edges in terms of weight, whereas the 1% visualizations in Fig. 5 each contain 548 edges.
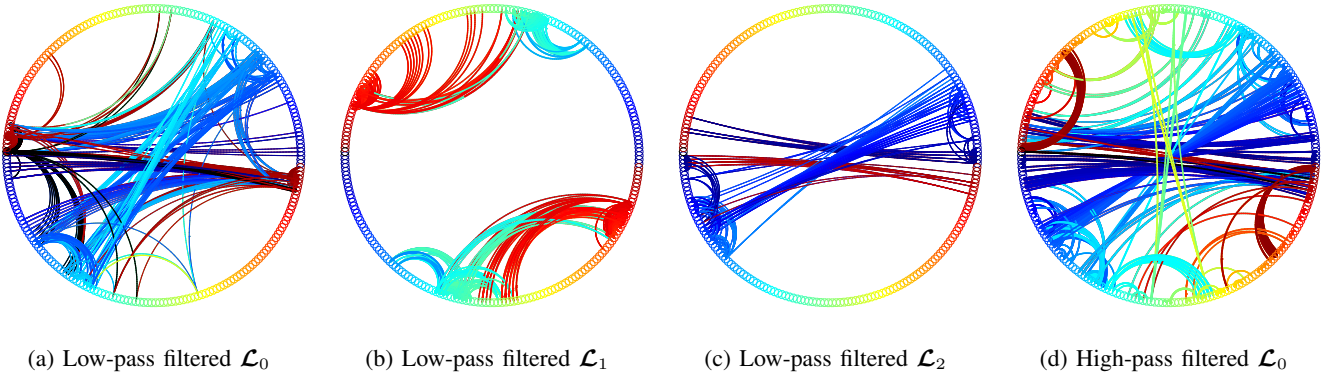
(a) Low-pass filtered $\mathcal{L}_0$ (b) Low-pass filtered $\mathcal{L}_1$ (c) Low-pass filtered $\mathcal{L}_2$ (d) High-pass filtered $\mathcal{L}_0$

Fig. 5: Depictions (1% visualizations) of the reconstructed adjacency structures after filtering.

Consider the following three Z-Laplacians as candidate shift operators:

$$\mathcal{L}_0 = D^{-1/2}(D - A)D^{-1/2} \tag{26}$$

$$\mathcal{L}_1 = D_W^{-1/2}[D_W - D^{-1}AD^{-1}]D_W^{-1/2} \tag{27}$$

$$\mathcal{L}_2 = Z^{1/2}D^{-1/2}(Z^{-1}D - A)D^{-1/2}Z^{1/2} . \tag{28}$$

These symmetric versions of the Z-Laplacian (Generalized Laplacians) are obtained through the similarity transformation (Lemma 3). The first shift operator, $\mathcal{L}_0$, is the symmetrized unbiased random walk Laplacian on the original adjacency. It is also the symmetric normalized Laplacian, which has been suggested as a shift operator [9]. The second shift operator, $\mathcal{L}_1$, represents the biased random walk in (25) with an increased tendency towards lower-degree vertices. The last shift operator, $\mathcal{L}_2$, is the Z-Laplacian representing a self-replicating process based on the unbiased random walk $\mathcal{L}_0$ but with $[Z]_{ii}$ set to 10 for vertices in the frontal lobe (blue) and 1 for other vertices. Thus, $\mathcal{L}_2$ emphasizes the hypothetical information flow associated with the frontal lobe. All three Z-Laplacian operators share the same uniform vertex time delays with $T = I$.

Following the approach of graph frequency analysis [9], [12], we consider the eigendecomposition

$$\mathcal{L} = V\Lambda V^T \tag{29}$$

of the Laplacians, where the columns of V are eigenvectors of $\mathcal{L}$ and Λ is a diagonal matrix comprising the corresponding eigenvalues. By replacing all but the four smallest eigenvalues with zero, we build simple low-pass filters based on the three different Z-Laplacian shift operators. The definition of high- and low-frequency bands is application specific. In this study, we choose the smallest four eigenpairs to be the low frequencies because we are interested in analyzing the structure of four major brain regions. We can demonstrate the effect of these filters by reconstructing the adjacency structures based on the original D and Z matrices:

$$A' = Z^{-1/2}D^{1/2}(I - V\Lambda'V^T)Z^{-1/2}D^{1/2} , \tag{30}$$

where Λ' contains the first four smallest eigenvalues on its diagonal, with all remaining elements set to zero.

The results are shown in Fig. 5, using 1% visualizations. Comparing Fig. 5(a) to Fig. 4, the high-frequency signals from $\mathcal{L}_0$ are filtered out, leaving mostly stronger cross-hemisphere connections. The filtered $\mathcal{L}_1$ network highlights distinctly different structures, with low-degree vertices from Fig. 4 now dominating the low-frequency spectrum. Strong cross-hemisphere connections associated with hub vertices are filtered out, revealing within-hemisphere connection patterns, especially those between parietal, occipital, and temporal lobes. In Fig. 5(c), the Z matrix is carefully designed to emphasize vertices in the frontal lobe. As expected, the result properly highlights the frontal lobe region and their internal connections, both within and across the hemispheres.

Finally, Fig. 5(d) depicts the effect of applying a high-pass filter obtained by replacing the four smallest eigenvalues of $\mathcal{L}_0$ with zero and leaving the rest unchanged. Comparing Figs. 5(a)–(d), we see that the different shift operators each produce unique patterns. Manipulating the Z-Laplacian allows exploration of different shift operators as we explore the brain connectivity. More importantly, the dynamical processes associated with each Z-Laplacian provides meaningful intuition and interpretations of the resulting shift operators and the induced family of linear invariant filters.

VII. CONCLUSIONS AND FUTURE WORK

In this paper, we proposed the *Z-Laplacian* framework, which is capable of modeling different discrete- and continuous-time dynamical processes on graphs, including diffusion and epidemic processes. We proved that the Z-Laplacian spans the space

of Z-matrices, leading to a general framework that unifies existing linear operators in the literature. When used as graph shift operators in applications, Z-Laplacian operators and their induced signal processing analysis have intuitive connections to the dynamical processes they model. This is especially useful for relating and comparing different aspects of the same topological structures.

The Z-Laplacian framework also naturally connects to concepts in network science, enabling graph theoretical methods to be used in signal processing problems. In particular, we showed a novel analysis that coupled network bottleneck discovery with the underlying wireless network protocol, including the impact of delay and collisions. We demonstrated how conductance can be used to find primary bottlenecks, whose location and effect may change with choice of MAC protocol, and we considered topology modifications to alleviate the bottleneck and heal the network. This leads to more general questions of the effects of protocols on network dynamical processes, such as consensus, as well as the study of resource allocation within the network, which are important issues for further study. We also showed how a variety of graph shift operators can be applied to the problem of structural brain connectivity frequency analysis. In the future, we plan to apply the GSP tools to functional brain signals. We will also investigate the mathematical properties of Z-Laplacians, unifying vertex centrality and community structure under the framework as we did previously for the *parameterized Laplacians* [10].

References

[1] M. Newman, *Networks: An Introduction*. New York: Oxford, 2010.

[2] P. Bonacich, "Power and centrality: a family of measures," *American J. Sociology*, vol. 92, pp. 1170–1182, March 1987.

[3] S. Fortunato, "Community detection in graphs," *Physics Reports*, vol. 486, pp. 75–174, Jan. 2010.

[4] S. P. Borgatti, "Centrality and network flow," *Social Networks*, vol. 27, pp. 55–71, Jan. 2005.

[5] R. Ghosh and K. Lerman, "Rethinking centrality: the role of dynamical processes in social network analysis," *Discrete Continuous Dynamical Syst. Series B*, vol. 19, pp. 1355–1372, July 2014.

[6] R. Ghosh, S.-H. Teng, K. Lerman, and X. Yan, "The interplay between dynamics and networks: centrality, communities, and Cheeger inequality," in *Proc. 20th ACM SIGKDD Int. Conf. Knowledge Discovery and Data Mining*, 2014, pp. 1406–1415.

[7] R. Olfati-Saber, J. A. Fax, and R. M. Murray, "Consensus and cooperation in networked multi-agent systems," *Proc. IEEE*, vol. 95, pp. 215–233, Jan. 2007.

[8] A. Sandryhaila and J. M. F. Moura, "Discrete signal processing on graphs," *IEEE Trans. Signal Process.*, vol. 61, pp. 1644–1656, Apr. 2013.

[9] D. I. Shuman, S. K. Narang, P. Frossard, A. Ortega, and P. Vandergheynst, "The emerging field of signal processing on graphs: extending high-dimensional data analysis to networks and other irregular data domains," *IEEE Sig. Processing Mag.*, vol. 61, pp. 1644–1656, Apr. 2013.

[10] X. Yan, S.-h. Teng, K. Lerman, and R. Ghosh, "Capturing the interplay of dynamics and networks through parameterizations of Laplacian operators," *PeerJ Computer Science*, vol. 2, e57, May 2016.

[11] M. Fiedler, *Special Matrices and Their Applications in Numerical Mathematics*. New York: Dover, 2008.

[12] A. Sandryhaila and J. M. Moura, "Discrete signal processing on graphs: frequency analysis," *IEEE Trans. Signal Process.*, vol. 62, pp. 3042–3054, Apr. 2014.

[13] A. Gavili and X.-P. Zhang, "On the shift operator, graph frequency and optimal filtering in graph signal processing," *ArXiv e-prints*, July 2017 [Online]. Available: https://arxiv.org/abs/1511.03512

[14] X. Yan, S.-H. Teng, and K. Lerman, "Multi-layer network composition under a unified dynamical process," *Lecture Notes in Computer Science*. vol. 10354, Springer, 2017.

[15] R. Lambiotte, J.-C. Delvenne, and M. Barahona, "Random walks, Markov processes and the multiscale modular organization of complex networks," *IEEE Trans. Netw. Sci. Eng.*, vol. 1, pp. 76–90, July–Dec. 2014.

[16] J. Gómez-Gardeñes and V. Latora, "Entropy rate of diffusion processes on complex networks," *Physical Review E*, vol. 78, 065102, Dec. 2008.

[17] Y. Wang, D. Chakrabarti, C. Wang, and C. Faloutsos, "Epidemic spreading in real networks: an eigenvalue viewpoint," in *Proc. 22nd Int. Symp. Reliable Distributed Systems*, 2003, pp. 25–34.

[18] A. Reibman and K. Trivedi, "Numerical transient analysis of Markov models," *Comput. Operations Research*, vol. 15, pp. 19–36, 1988.

[19] D. Taylor, S. A. Myers, A. Clauset, M. A. Porter, and P. J. Mucha, "Eigenvector-based centrality measures for temporal networks," *Multiscale Modeling Simulation*, vol. 15, pp. 537–574, March 2017.

[20] E. Pavez and A. Ortega, "Generalized Laplacian precision matrix estimation for graph signal processing," in *2016 IEEE Int. Conf. Acoustics, Speech Signal Process.*, 2016, pp. 6350–6354.

[21] M. X. Cheng, Y. Ling, and B. M. Sadler, "Wireless ad hoc networks connectivity assessment and relay node deployment," in *2014 IEEE Global Commun. Conf.*, pp. 399–404.

[22] M. X. Cheng, Y. Ling, and B. M. Sadler, "Network connectivity assessment and improvement through relay node deployment," *Theoretical Comput. Sci.*, vol. 660, pp. 86–101, Jan. 2017.

[23] R. F. Betzel, A. Griffa, A. Avena-Koenigsberger, J. Goñi, J.-P. Thiran, P. Hagmann, and O. Sporns, "Multi-scale community organization of the human structural connectome and its relationship with resting-state functional connectivity," *Netw. Sci.*, vol. 1, pp. 353–373, Dec. 2013.

[24] W. Huang, L. Goldsberry, N. F. Wymbs, S. T. Grafton, D. S. Bassett, and A. Ribeiro, "Graph frequency analysis of brain signals," *IEEE J. Selected Topics Signal Process.*, vol. 10, pp. 1189–1203, Oct. 2016.

[25] S. Mowlaei, A. Singh, and A. Ghuman, "Frequency bands are an organizational force of intrinsic brain networks," *Soc. Neuroscience*, 2016.

[26] M. Daianu, A. Mezher, N. Jahanshad, D. P. Hibar, T. M. Nir, C. R. Jack, M. W. Weiner, M. A. Bernstein, and P. M. Thompson, "Spectral graph theory and graph energy metrics show evidence for the Alzheimer's disease disconnection syndrome in APOE-4 risk gene carriers," *2015 IEEE 12th Int. Symp. Biomedical Imaging*, 2015, pp. 458–461.

[27] J. D. Medaglia, W. Huang, E. A. Karuza, S. L. Thompson-Schill, A. Ribeiro, and D. S. Bassett, "Functional alignment with anatomical networks is associated with cognitive flexibility," *ArXiv e-prints*, Nov. 2016 [Online]. Available: https://arxiv.org/abs/1611.08751

[28] M. Daianu, G. Ver Steeg, A. Mezher, N. Jahanshad, T. M. Nir, X. Yan, G. Prasad, K. Lerman, A. Galstyan, and P. M. Thompson, "Information-theoretic clustering of neuroimaging metrics related to cognitive decline in the elderly," *Lecture Notes in Computer Science*. vol. 9601, Springer, 2016, pp. 13–23.

[29] A. Irimia, M. C. Chambers, C. M. Torgerson, and J. D. Van, "Circular representation of human cortical networks for subject and population-level connectomic visualization," *Neuroimage*, vol. 60, pp. 1340–1351, April 2012.

A. Proof of Lemma 1

Lemma (Bias transformation). *Any biased random walk on $G = (V, E, \boldsymbol{A})$, with the diagonal matrix $\boldsymbol{B}$ specifying vertex bias factors b_v, is equivalent to an unbiased random walk on the transformed graph $\boldsymbol{W} = \boldsymbol{AB}$. If G is undirected, then we instead consider he transformed graph $\boldsymbol{W} = \boldsymbol{BAB}$ to maintain edges having equal weight in both directions.*

Proof. Given the transformed graph $\boldsymbol{W}$, the transition probability of an unbiased random walk going from vertex u to vertex v is defined as

$$\boldsymbol{P}'_{uv} = [\boldsymbol{D_W}_{\text{out}}^{-1}\boldsymbol{W}]_{uv} = \frac{\boldsymbol{W}_{uv}}{\sum_v \boldsymbol{W}_{uv}} \propto b_v a_{uv} , \tag{31}$$

which is equivalent to the transition probability $P_{uv}^{\text{BRW}} \propto b_v a_{uv}$ of the biased random walk on the original adjacency matrix $\boldsymbol{A}$.

For an undirected graph, we need to guarantee the transition probabilities are preserved in both directions. Given $\boldsymbol{W} = \boldsymbol{BAB}$, we have

$$\begin{aligned}
\boldsymbol{P}'_{uv} &= [\boldsymbol{D_W}^{-1}\boldsymbol{W}]_{uv} = \frac{\boldsymbol{W}_{uv}}{\sum_v \boldsymbol{W}_{uv}} \propto \frac{b_v a_{uv} b_u}{b_u} \propto P_{uv}^{\text{BRW}} \\
\boldsymbol{P}'_{vu} &= [\boldsymbol{D_W}^{-1}\boldsymbol{W}]_{vu} = \frac{\boldsymbol{W}_{vu}}{\sum_u \boldsymbol{W}_{uv}} \propto \frac{b_v a_{vu} b_u}{b_v} \propto P_{vu}^{\text{BRW}} .
\end{aligned} \tag{32}$$

$\square$

B. Proof of Lemma 2

Lemma (Delay transformation). *Any unbiased continuous-time random walk on $G = (V, E, \boldsymbol{A})$, with the diagonal matrix $\boldsymbol{T}$ specifying vertex delay factors τ_v, is equivalent to a continuous-time random walk with delay factors $\boldsymbol{I}$ on the transformed graph $\boldsymbol{W} = \boldsymbol{D}_{out}(\boldsymbol{T} - \boldsymbol{I}) + \boldsymbol{A}$.*

Proof. Starting from the unbiased random walk Laplacian with the delay factors $\boldsymbol{T}$, we have

$$\begin{aligned}
\boldsymbol{T}^{-1}\boldsymbol{D}_{\text{out}}^{-1}(\boldsymbol{D}_{\text{out}} - \boldsymbol{A}) &= \boldsymbol{I}\boldsymbol{T}^{-1} - \boldsymbol{T}^{-1}\boldsymbol{D}_{\text{out}}^{-1}\boldsymbol{A} \\
&= \boldsymbol{I} - \boldsymbol{T}^{-1}(\boldsymbol{T} - \boldsymbol{I} + \boldsymbol{D}_{\text{out}}^{-1}\boldsymbol{A}) \\
&= \boldsymbol{D_W}_{\text{out}}^{-1}\boldsymbol{D_W}_{\text{out}}(\boldsymbol{I} - \boldsymbol{T}^{-1}(\boldsymbol{T} - \boldsymbol{I}) - \boldsymbol{T}^{-1}\boldsymbol{D}_{\text{out}}^{-1}\boldsymbol{A}) \\
&= \boldsymbol{D_W}_{\text{out}}^{-1}(\boldsymbol{D_W}_{\text{out}} - \boldsymbol{D}_{\text{out}}(\boldsymbol{T} - \boldsymbol{I}) - \boldsymbol{A}) \\
&= \boldsymbol{I}\boldsymbol{D_W}_{\text{out}}^{-1}(\boldsymbol{D_W}_{\text{out}} - \boldsymbol{W}) ,
\end{aligned} \tag{33}$$

where the new transformed matrix is $\boldsymbol{W} = \boldsymbol{D}_{\text{out}}(\boldsymbol{T} - \boldsymbol{I}) + \boldsymbol{A}$ and $\boldsymbol{D_W}_{\text{out}}$ represents its diagonal out-degree matrix. $\square$

C. Proof of Lemma 6

Lemma (Discrete approximation). *Given the graph signal $\boldsymbol{\theta}(t)$ and the continuous-time Z-Laplacian $\boldsymbol{T}^{-1}(\boldsymbol{I} - \boldsymbol{Z}\boldsymbol{D}_{out}^{-1}\boldsymbol{A})$, the graph signal at time $t + \delta$ can be approximated as $\delta \to 0$ by*

$$\lim_{\delta \to 0} \boldsymbol{\theta}(t + \delta) = \boldsymbol{\theta}(t)e^{-\boldsymbol{\mathcal{L}}\delta} = \boldsymbol{\theta}(t)(\boldsymbol{I} - \lim_{\delta \to 0} \delta\boldsymbol{\mathcal{L}}) ,$$

where $\boldsymbol{I} - \delta\boldsymbol{\mathcal{L}}$ represents a discrete-time filter.

Proof. To better illustrate the role and impact of $\boldsymbol{T}$ in the continuous version of the general nonnegative filter, we focus on the dynamics of a specific vertex u over a time interval δ, given by

$$\begin{aligned}
[\boldsymbol{\theta}(t + \delta) - \boldsymbol{\theta}(t)]_u &= [\boldsymbol{\theta}(t)(e^{-\boldsymbol{\mathcal{L}}\delta} - \boldsymbol{I})]_u \\
&= -[\boldsymbol{\theta}(t)]_u + \sum_v [\boldsymbol{\theta}(t)]_v \left[e^{-\lambda\delta} \sum_{k=0}^{\infty} \frac{1}{k!}(\lambda\boldsymbol{\Phi}\delta)^k \right]_{vu} ,
\end{aligned} \tag{34}$$

where $\boldsymbol{\Phi} = \boldsymbol{I} - \frac{1}{\lambda}\boldsymbol{\mathcal{L}}$ is a discrete-time filter. For small δ, we have

$$
\begin{aligned}
[\boldsymbol{\theta}(t+\delta) &- \boldsymbol{\theta}(t)]_u \\
&= -[\boldsymbol{\theta}(t)]_u + \sum_v [\boldsymbol{\theta}(t)]_v \left[e^{-\lambda\delta}(\boldsymbol{I} + \lambda\boldsymbol{\Phi}\delta + O(\delta^2)) \right]_{vu} \\
&\approx -[\boldsymbol{\theta}(t)]_u + e^{-\lambda\delta} \sum_v [\boldsymbol{\theta}(t)]_v \left[\boldsymbol{I} + \lambda(\boldsymbol{I} - \frac{1}{\lambda}\boldsymbol{\mathcal{L}})\delta \right]_{vu} \\
&= \left(e^{-\lambda\delta}(1 + \lambda\delta) - 1 \right)[\boldsymbol{\theta}(t)]_u - e^{-\lambda\delta} \sum_v [\boldsymbol{\theta}(t)]_v \, [\delta\boldsymbol{\mathcal{L}}]_{vu} \ ,
\end{aligned}
\tag{35}
$$

where in the first equality we use the *Big-O* notation to capture the asymptotically shrinking quadratic and higher-order terms of δ. Therefore,

$$
\begin{aligned}
\frac{[\boldsymbol{\theta}(t+\delta) - \boldsymbol{\theta}(t)]_u}{\delta} \\
\approx \left(\frac{e^{-\lambda\delta} - 1}{\delta} + \lambda e^{-\lambda\delta} \right)[\boldsymbol{\theta}(t)]_u - e^{-\lambda\delta} \sum_v [\boldsymbol{\theta}(t)]_v \, [\boldsymbol{\mathcal{L}}]_{vu} \ .
\end{aligned}
\tag{36}
$$

It follows that, in the limit of $\delta \to 0$, (36) approaches the differential equation (16):

$$
\lim_{\delta \to 0} \frac{[\boldsymbol{\theta}(t+\delta) - \boldsymbol{\theta}(t)]_u}{\delta} = -\sum_v [\boldsymbol{\theta}(t)]_v \, [\boldsymbol{\mathcal{L}}]_{vu} = \left[\frac{d\boldsymbol{\theta}(t)}{dt} \right]_u \ .
\tag{37}
$$

Rearranging terms,

$$
\begin{aligned}
\lim_{\delta \to 0} [\boldsymbol{\theta}(t+\delta)]_u &= \lim_{\delta \to 0} [-\boldsymbol{\theta}(t)\delta\boldsymbol{\mathcal{L}} + \boldsymbol{\theta}(t)]_u \\
&= \lim_{\delta \to 0} [\boldsymbol{\theta}(t)(1 - \delta\boldsymbol{\mathcal{L}})]_u \ ,
\end{aligned}
\tag{38}
$$

and

$$
\lim_{\delta \to 0} \boldsymbol{\theta}(t+\delta) = \boldsymbol{\theta}(t)(\boldsymbol{I} - \lim_{\delta \to 0} \delta\boldsymbol{\mathcal{L}}) \ ,
\tag{39}
$$

where the discrete-time filter $\boldsymbol{I} - \lim_{\delta \to 0} \delta\boldsymbol{\mathcal{L}}$ becomes a close approximation to the continuous-time filter. $\qquad\square$

D. Proof of Theorem 3

Theorem (Delay interpretation)**.** *Given the continuous-time Z-Laplacian $\boldsymbol{T}^{-1}(\boldsymbol{I} - \boldsymbol{Z}\boldsymbol{D}_{\mathrm{out}}^{-1}\boldsymbol{A})$ and its discrete-time approximation $\boldsymbol{\Phi}$, the delay factor $[\boldsymbol{T}]_{uu}$ of vertex u is proportional to the expected "waiting steps" on vertex u for the approximated discrete-time random walk.*

Proof. We rewrite the discrete-time filter $\boldsymbol{\Phi}$ as

$$
\begin{aligned}
\boldsymbol{\Phi} &= \boldsymbol{I} - \delta\boldsymbol{T}^{-1}(\boldsymbol{I} - \boldsymbol{Z}\boldsymbol{D}_{\mathrm{out}}^{-1}\boldsymbol{A}) \\
&= (\boldsymbol{I} - \delta\boldsymbol{T}^{-1}) + \delta\boldsymbol{T}^{-1}\boldsymbol{Z}\boldsymbol{D}_{\mathrm{out}}^{-1}\boldsymbol{A} \ .
\end{aligned}
\tag{40}
$$

Without loss of generality, we assume that $\tau_i \leq 1$ for all diagonal entries τ_i of $\boldsymbol{T}$. Setting $\delta = \min_i \tau_i$, it follows that the second term of (40) represents a row-wise downscaling of the original expression $\boldsymbol{Z}\boldsymbol{D}_{\mathrm{out}}^{-1}\boldsymbol{A}$, which can be rewritten as a new discrete-time filter given by

$$
\delta\boldsymbol{T}^{-1}\boldsymbol{Z}\boldsymbol{D}_{\mathrm{out}}^{-1}\boldsymbol{A} = \boldsymbol{Z}'\boldsymbol{D}_{\mathrm{out}}^{-1}\boldsymbol{A} \ .
\tag{41}
$$

The first term of (40), $\boldsymbol{I} - \delta\boldsymbol{T}^{-1}$, with all entries in the real interval $[0, 1)$, represents probabilities of self-looping random walks at each vertex. Since this is equivalent to staying at the same vertex with no dynamics, we can estimate the expected "waiting steps" at vertex v to be

$$
\sum_{k=0}^{\infty} \left(1 - \frac{\delta}{\tau_v} \right)^k = \frac{1}{\delta/\tau_v} = \frac{\tau_v}{\min_i \tau_i} \ ,
\tag{42}
$$

and so τ_v is the "delay factor" of vertex v. $\qquad\square$